DEMOSAICKING USING VECTOR SPECTRAL MODEL

Rastislav Lukac and Konstantinos N. Plataniotis

Multimedia Laboratory - BA 4157, The Edward S. Rogers Sr. Department of ECE,
University of Toronto, 10 King's College Road, Toronto, Canada
lukacr@ieee.org, kostas@dsp.utoronto.ca

ABSTRACT

A new edge-sensing demosaicking solution based on a novel vector spectral model is introduced in this paper. Using the vector spectral model, the proposed solution preserves the magnitude and the directional characteristics of the single-sensor captured image in both smooth and edge areas. Experimentation reported in this paper indicates that the proposed demosaicking solution produces visually pleasing color images and can outperform the powerful demosaicking schemes in terms of the performance.

1. INTRODUCTION

Single-sensor digital cameras use a color filter array (CFA) placed on top of a monochrome image sensor, usually a charge-coupled device (CCD) or complementary metal oxide semiconductor (CMOS) sensor, to capture the visual scene [1]-[5]. Since each sensor cell has its own spectrally selective filter, the acquired CFA data constitutes a mosaic-like, gray-scale image [5]. The missing color components at each spatial location of the acquired CFA image are estimated using a demosaicking process which produces a full-color demosaicked image [3]-[9].

This paper introduces a new demosaicking solution. The proposed solution uses an edge-sensing mechanism to preserve the structural content (edges and fine details) of the captured image and avoid edge blurring. More importantly, our solution uses a novel vector spectral model introduced in [10] to follow the spectral characteristics of the true visual scene and produce visually pleasing demosaicked full-color images without color shifts and artifacts. Note that our previous work [10] focuses on the introduction and analysis of the vector spectral model. The performance issues will be addressed in this paper.

2. VECTOR SPECTRAL MODEL

It is well-known [11]-[13] that natural images consist of small regions which exhibit similar, if not identical, color-chromaticity properties and that color chromaticity relates to the directional characteristics of color vectors. Two color vectors $\mathbf{x}_{(r,s)} = [x_{(r,s)1}, x_{(r,s)2}, x_{(r,s)3}]$ and $\mathbf{x}_{(i,j)} = [x_{(i,j)1}, x_{(i,j)2}, x_{(i,j)3}]$ occupying spatially neighboring locations (r,s) and (i,j) have the same chromaticity characteristics if they are collinear in the RGB color space [10], resulting in $\langle \mathbf{x}_{(r,s)}, \mathbf{x}_{(i,j)} \rangle = 0$ with $\langle \mathbf{x}_{(r,s)}, \mathbf{x}_{(i,j)} \rangle$ denoting the angle between $\mathbf{x}_{(r,s)}$ and $\mathbf{x}_{(i,j)}$. Thus, the enforcement of orientation constraints implies the following:

$$\frac{\sum_{k=1}^{3} x_{(r,s)k} x_{(i,j)k}}{\sqrt{\sum_{k=1}^{3} x_{(r,s)k}^2} \sqrt{\sum_{k=1}^{3} x_{(i,j)k}^2}} = 1 \qquad (1)$$

Fig. 1. Bayer CFA [14].

Since both the magnitude and directional characteristics of the color vectors are essential for the human perception, the magnitude information is incorporated into the vector model via the constraint $\langle \mathbf{x}_{(r,s)} + \gamma \mathbf{1}, \mathbf{x}_{(i,j)} + \gamma \mathbf{1} \rangle = 0$. The vectors $[\mathbf{x}_{(\cdot,\cdot)} + \gamma \mathbf{1}] = [x_{(\cdot,\cdot)1} + \gamma, x_{(\cdot,\cdot)2} + \gamma, x_{(\cdot,\cdot)3} + \gamma]$ obtained using the vector $\mathbf{1} = [1, 1, 1]$ and the parameter γ are linearly shifted variants of the input vectors $\mathbf{x}_{(\cdot,\cdot)}$ of proper dimensions. In this case, the enforcement of the orientation constraints implies the following:

$$\frac{\sum_{k=1}^{3} (x_{(r,s)k} + \gamma)(x_{(i,j)k} + \gamma)}{\sqrt{\sum_{k=1}^{3} (x_{(r,s)k} + \gamma)^2} \sqrt{\sum_{k=1}^{3} (x_{(i,j)k} + \gamma)^2}} = 1 \qquad (2)$$

where the parameter γ is used to control the influence of both the directional and the magnitude characteristics of the neighboring vectors during processing. The scale shift introduced by the parameter γ prevents color shifts in flat areas as well as near edge transitions. A number of processing solutions, with different design characteristics and performance, can be thus obtained by modifying γ. In addition, the vector model in (2) generalizes previous spectral models in [15]-[18]. The interested reader can find extensive analysis of the vector spectral model in [10].

Using (2), any component $x_{(r,s)k}$ of the color vector $\mathbf{x}_{(r,s)}$ can be determined based on the available neighboring vector $\mathbf{x}_{(i,j)}$ and the remaining components of $\mathbf{x}_{(r,s)}$. As proven in [10], the approach always leads to the quadratic equation with a unique solution (both roots identical). Assuming that the R ($k = 1$), G ($k = 2$), or B ($k = 3$) component $y_{(r,s)}^{(i,j)} = x_{(r,s)k}$ is being determined via (2), the solution can be obtained using (3), (4), or (5), respectively. Through the inverse shifting via $-\gamma$ in these equations, the procedure outputs a color component in the appropriate dynamic range.

Note that each of (3)-(5) can be reduced to a two-dimensional expression by putting the color components in one of the color channels to zero. Such an approach is appropriate when an RGB vector field is incomplete and only two-dimensional vectors, mostly RG or

$$y_{(r,s)}^{(i,j)} = -\gamma + \frac{(x_{(r,s)2}+\gamma)(x_{(i,j)1}+\gamma)(x_{(i,j)2}+\gamma) + (x_{(r,s)3}+\gamma)(x_{(i,j)1}+\gamma)(x_{(i,j)3}+\gamma)}{(x_{(i,j)2}+\gamma)^2 + (x_{(i,j)3}+\gamma)^2} \qquad (3)$$

$$y_{(r,s)}^{(i,j)} = -\gamma + \frac{(x_{(r,s)1}+\gamma)(x_{(i,j)1}+\gamma)(x_{(i,j)2}+\gamma) + (x_{(r,s)3}+\gamma)(x_{(i,j)2}+\gamma)(x_{(i,j)3}+\gamma)}{(x_{(i,j)1}+\gamma)^2 + (x_{(i,j)3}+\gamma)^2} \qquad (4)$$

$$y_{(r,s)}^{(i,j)} = -\gamma + \frac{(x_{(r,s)1}+\gamma)(x_{(i,j)1}+\gamma)(x_{(i,j)3}+\gamma) + (x_{(r,s)2}+\gamma)(x_{(i,j)2}+\gamma)(x_{(i,j)3}+\gamma)}{(x_{(i,j)1}+\gamma)^2 + (x_{(i,j)2}+\gamma)^2} \qquad (5)$$

BG vectors due to the double frequency of G locations in the Bayer CFA (*Fig.1*), can be constituted during processing. In this case, the missing R (for $k = 1$) or B (for $k = 3$) component $y_{(r,s)}^{(i,j)} = x_{(r,s)k}$ is given by:

$$y_{(r,s)}^{(i,j)} = -\gamma + (x_{(r,s)2}+\gamma)(x_{(i,j)k}+\gamma)/(x_{(i,j)2}+\gamma) \qquad (6)$$

Similarly, the G component $y_{(r,s)}^{(i,j)} = x_{(r,s)2}$ can be expressed using the available R ($k = 1$) or B ($k = 3$) components $x_{(\cdot,\cdot)k}$ and the neighboring G component $x_{(i,j)2}$ as follows:

$$y_{(r,s)}^{(i,j)} = -\gamma + (x_{(r,s)k}+\gamma)(x_{(i,j)2}+\gamma)/(x_{(i,j)k}+\gamma) \qquad (7)$$

3. PROPOSED DEMOSAICKING METHOD

To overcome the spatial, structural and spectral limitations of the image formation and color reconstruction phases, the proposed solution uses a spectral model and an edge-sensing mechanisms to follow the spectral and structural characteristics of the captured image in a localized neighborhood described by ζ. Since the CFA image has a mosaic-like structure and not all of the neighboring locations correspond to a color channel being reconstructed, operating on the image $\mathbf{x}$ obtained using the well-known Bayer CFA the parameter ζ is most commonly limited to the shape-masks $\zeta = \{(r-1,s),(r,s-1),(r,s+1),(r+1,s)\}$ shown in *Fig.2a* and $\zeta = \{(r-1,s-1),(r-1,s+1),(r+1,s-1),(r+1,s+1)\}$ shown in *Fig.2b*.

Using the data-adaptive concept in [5] and the vector spectral model in (2), the proposed method quantifies the contributions of the adjacent color vectors $\mathbf{x}_{(i,j)}$ inside ζ to the vector $\mathbf{x}_{(r,s)}$ under consideration as follows [5]:

$$x_{(r,s)k} = \sum_{(i,j)\in\zeta} \{w'_{(i,j)} y_{(r,s)}^{(i,j)}(\mathbf{x}_{(r,s)}, \mathbf{x}_{(i,j)}, \gamma)\} \qquad (8)$$

where $y_{(r,s)}^{(i,j)}(\mathbf{x}_{(r,s)}, \mathbf{x}_{(i,j)}, \gamma)$ is a function enforcing the modelling constraints in (2), whereas the term $(i,j) \in \zeta$ denotes the spatial location arrangements on the image lattice. Each of the available color vectors $\mathbf{x}_{(i,j)}$ inside ζ is associated with the normalized weighting coefficient $w'_{(i,j)}$ defined as $w'_{(i,j)} = w_{(i,j)}/\sum_{(i,j)\in\zeta} w_{(i,j)}$, where $w_{(i,j)}$ are the so-called edge-sensing weights used to direct the processing along the natural edges in the true image. This operation preserves the structural image content and produces a sharply looking demosaicked image. Note that following the discussion in [10], $\gamma = 256$ is used throughout this paper.

To develop the computationally efficient solution, the proposed method uses a simple edge-sensing mechanism of [6]. The weights $w_{(i,j)}$, for $(i,j) \in \zeta$, are calculated for a diamond-shape mask $\zeta = \{(r-1,s),(r,s-1),(r,s+1),(r+1,s)\}$ in (8) using the original CFA components $z_{(\cdot,\cdot)}$ as follows:

$$\begin{aligned} w_{(r-1,s)} &= [1+|z_{(r-2,s)}-z_{(r,s)}|+|z_{(r-1,s)}-z_{(r+1,s)}|]^{-1} \\ w_{(r,s-1)} &= [1+|z_{(r,s-2)}-z_{(r,s)}|+|z_{(r,s-1)}-z_{(r,s+1)}|]^{-1} \\ w_{(r,s+1)} &= [1+|z_{(r,s+2)}-z_{(r,s)}|+|z_{(r,s+1)}-z_{(r,s-1)}|]^{-1} \\ w_{(r+1,s)} &= [1+|z_{(r+2,s)}-z_{(r,s)}|+|z_{(r+1,s)}-z_{(r-1,s)}|]^{-1} \end{aligned} \qquad (9)$$
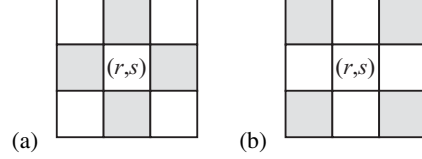

Fig. 2. Shape masks used in the proposed method: (a) $\zeta = \{(r-1,s),(r,s-1),(r,s+1),(r+1,s)\}$, (b) $\zeta = \{(r-1,s-1),(r-1,s+1),(r+1,s-1),(r+1,s+1)\}$.

Otherwise, a square-shape mask $\zeta = \{(r-1,s-1),(r-1,s+1),(r+1,s-1),(r+1,s+1)\}$ is considered, with the weights given by:

$$\begin{aligned} w_{(r-1,s-1)} &= [1+|z_{(r-2,s-2)}-z_{(r,s)}|+|z_{(r-1,s-1)}-z_{(r+1,s+1)}|]^{-1} \\ w_{(r-1,s+1)} &= [1+|z_{(r-2,s+2)}-z_{(r,s)}|+|z_{(r-1,s+1)}-z_{(r+1,s-1)}|]^{-1} \\ w_{(r+1,s-1)} &= [1+|z_{(r+2,s-2)}-z_{(r,s)}|+|z_{(r+1,s-1)}-z_{(r-1,s+1)}|]^{-1} \\ w_{(r+1,s+1)} &= [1+|z_{(r+2,s+2)}-z_{(r,s)}|+|z_{(r+1,s+1)}-z_{(r-1,s-1)}|]^{-1} \end{aligned} \qquad (10)$$

To this end, the proposed demosaicking procedure can be summarized as follows. Acquiring the CFA data constitutes a $K_1 \times K_2$ gray-scale mosaic-like image $z : Z^2 \to Z$ with the pixels $z_{(r,s)}$ occupying the spatial location (r,s) which is denoted by the row and column coordinates $r = 1, 2, ..., K_1$ and $s = 1, 2, ..., K_2$. Using a widely accepted Bayer CFA with the GRGR phase in the first row (*Fig.1*) [14], the acquired CFA image z can be transformed to its $K_1 \times K_2$ low resolution color variant $\mathbf{x} : Z^2 \to Z^3$ with the vectorial pixels $\mathbf{x}_{(r,s)} = [x_{(r,s)1}, x_{(r,s)2}, x_{(r,s)3}]$. The transformation forms $\mathbf{x}_{(r,s)} = [z_{(r,s)}, 0, 0]$ for (odd r, even s), $\mathbf{x}_{(r,s)} = [0, z_{(r,s)}, 0]$ for (odd r, odd s) and (even r, even s), and $\mathbf{x}_{(r,s)} = [0, 0, z_{(r,s)}]$ for (even r, odd s). Since the sensor acquires only one value per spatial location, the missing components $x_{(r,s)k}$ in the vectors $\mathbf{x}_{(r,s)}$ are equal to zeros to denote their portion to the coloration of $\mathbf{x}_{(r,s)}$.

Operating on the image $\mathbf{x}$, the proposed demosaicking solution populates the G color plane using (8) with $\zeta = \{(r-1,s),(r,s-1),(r,s+1),(r+1,s)\}$, (7) and (9). The required spectral information in (7) is obtained through the predicted R ($k = 1$) or B ($k = 3$) values $x_{(i,j)k}$ obtained for $(i,j) \in \zeta$ as $x_{(r-1,s)k} = (z_{(r,s)}+z_{(r-2,s)})/2$, $x_{(r,s-1)k} = (z_{(r,s)}+z_{(r,s-2)})/2$, $x_{(r,s+1)k} = (z_{(r,s)}+z_{(r,s+2)})/2$, and $x_{(r+1,s)k} = (z_{(r,s)}+z_{(r+2,s)})/2$. The parameter $k = 1$ or $k = 3$ corresponds respectively to the original R or B CFA component located at (r,s). After producing the G components $x_{(r,s)2}$, the predicted R and B values are discarded.

In the next step, the R ($k = 1$) and B ($k = 3$) color planes are fully populated using (8) with $\zeta = \{(r-1,s-1),(r-1,s+1),(r+1,s-1),(r+1,s+1)\}$ and (10), and then with $\zeta = \{(r-1,s),(r,s-1),(r,s+1),(r+1,s)\}$ and (9). The components $y_{(r,s)}^{(i,j)}(\cdot)$ in (8) are obtained using (6). Although this processing step produces a full-color demosaicked image, the desired highest visual quality is obtained in the next two steps.

Since the previous processing steps fully populated the array of three-component RGB vectors, the previously obtained G color components $x_{(r,s)2}$ are re-calculated using (8) with (4), (9) and $\zeta = \{(r-1,s),(r,s-1),(r,s+1),(r+1,s)\}$.

Fig. 3. Test color images: (a) Mountains, (b) Bird, (c) Celebration, (d) Butterfly, (e) Woman, (f) Parrothead.

Table 1. Objective evaluation using the averaged results corresponding to the image database shown in *Fig.3*.

Method	MAE	MSE	NCD	SCD
[3]	2.983	37.936	0.0716	1.6148
[4]	2.560	29.040	0.0613	1.5236
[5]	2.863	35.100	0.0687	1.7098
[6]	2.620	29.341	0.0624	1.5771
[7]	2.585	28.520	0.0624	1.5070
[8]	2.713	31.901	0.0660	1.4621
[9]	2.615	30.678	0.0612	1.6550
Proposed	2.456	25.786	0.0584	1.4593

Similarly, the previously obtained R ($k = 1$) and B ($k = 3$) color components $x_{(r,s)k}$ are re-calculated using (8) with (3) and (5), respectively, to eliminate visual impairments. This processing step uses first $\zeta = \{(r-1, s-1), (r-1, s+1), (r+1, s-1), (r+1, s+1)\}$ and (10) to denote the required inputs in (8). Then, the proposed method completes with (8) based on $\zeta = \{(r-1, s), (r, s-1), (r, s+1), (r+1, s)\}$ and (9).

4. EXPERIMENTAL RESULTS

To determine the performance of the proposed demosaicking solution, a number of test images have been utilized. Examples such as the 512×512 test color images shown in *Fig.3* are used to emulate the processing scenario. These test images, which vary in color appearance and in the complexity of the structural content (edges), have been captured using three-sensor devices and normalized to 8-bit per channel RGB representation.

Following the standard practice previously reported in [3]-[5], the tests were performed by sampling the original images (*Fig.3*) with a GRGR-phased Bayer CFA filter (*Fig.2*) to obtain a CFA image z. The pixels $z_{(r,s)}$ in the image z were generated using $z_{(r,s)} = o_{(r,s)1}$ for r odd and s even, $z_{(r,s)} = o_{(r,s)3}$ for r even and s odd, and finally $z_{(r,s)} = o_{(r,s)2}$ in all remaining locations. The term $o_{(r,s)k}$ denotes the R ($k = 1$), G ($k = 2$) and B ($k = 3$) component of the original color vector $\mathbf{o}_{(r,s)} = [o_{(r,s)1}, o_{(r,s)2}, o_{(r,s)3}]$ with $r = 1, 2, ..., K_1$ and $s = 1, 2, ..., K_2$. The demosaicked images $\mathbf{x}$ are obtained by applying the demosaicking solution to the CFA image z. To facilitate the objective comparisons, the RGB color space based mean absolute error (MAE) and mean square error (MSE) criteria [5], the CIE-LUV color space based normalized color difference (NCD) criterion [5], and the spatial color difference (SCD) criterion defined in the S-CIELab color space [19] are used to measure the difference between the original color image $\mathbf{o}$ and the demosaicked image $\mathbf{x}$. In the experiments reported here, the proposed demosaicking solution was compared against the powerful demosaicking schemes presented in [3]-[9].

Demosaicking results reported in *Table 1* are calculated as aggregated measures averaged over the number of images in the test database (*Fig.3*). Therefore, these results can be considered a good indicator of the robustness of the demosaicking schemes. As it can
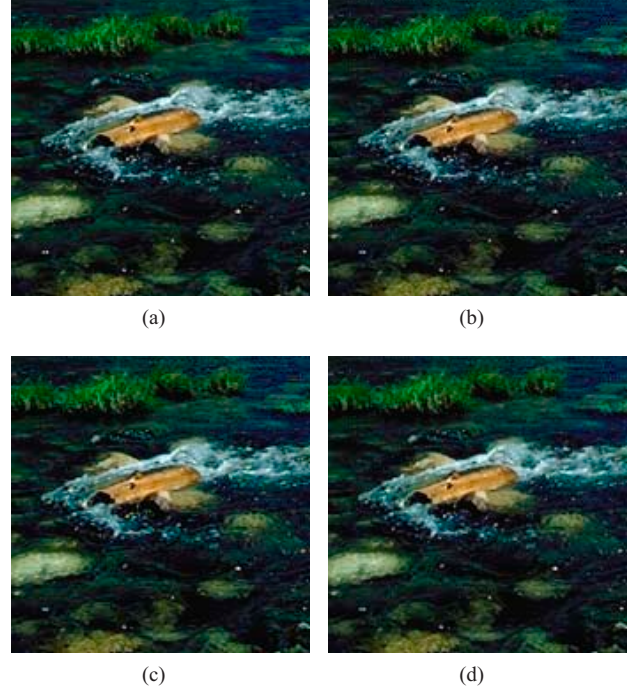

Fig. 4. Enlarged parts of the Mountains image: (a) original image, (b) method in [3], (c) method in [8], (d) proposed method.

be seen from the reported numbers, the proposed solution outperforms other demosaicking schemes with respect to all objective criteria. Additional improvements in performance are expected, as part of our future work, through: i) the replacement of the simple edge-sensing mechanism in (9)-(10) with other more sophisticated designs, and ii) the introduction of a locally adaptive control of γ.

Figs.4-6 depict enlarged parts of the test images cropped in areas with high edge density. The results allow for the visual comparison of the considered methods. Demosaicked results produced by the proposed solution indicate higher visual quality compared to the results obtained using other schemes. The solutions in [3],[5],[6] preserve color/structural information, however, they often introduce visually annoying zipper effects. Although other methods, such as those described in [4],[8] usually avoid zipper effects, they produce the images with color shifts. This is not the case when the proposed solution is used. The undesired effects are either completely removed or significantly reduced by our solution which excellently operates in all areas of the image producing a demosaicked output with excellent fidelity in both color and structure.

Apart from the numerical behavior (actual performance) of the proposed solution, its computational complexity should be carefully examined as it is a realistic measure of its practicality and usefulness. The efficiency of the proposed solution was measured, in terms of execution time, using a conventional PC with a standard operating system and programming environment. When implemented in software, the execution of the proposed demosaicking tool on an Intel Pentium IV 2.40 GHz CPU, 512 MB RAM box with Windows XP operating system and MS Visual C^{++} 5.0 programming environment, took (on average) 1.753 s to demosaick a 512×512 CFA image. The recorded value suggests that the proposed demosaicking method is computationally efficient.

Fig. 6. Enlarged parts of the Parrothead image: (a) original image, (b) method in [3], (c) method in [8], (e) proposed method.
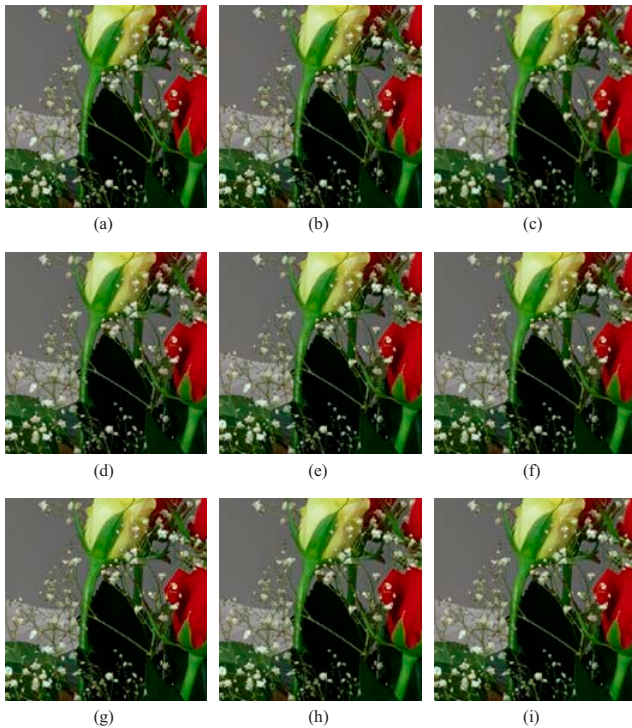
Fig. 5. Enlarged parts of the Woman image: (a) original image, (b) method in [3], (c) method in [4], (d) method in [5], (e) method in [6], (f) method in [7], (g) [8], (h) method in [9], (i) proposed method.

5. CONCLUSION

A powerful demosaicking solution was introduced in this work. A novel vector spectral model was used to boost the performance of the edge-sensing demosaicking process. Following the spectral, structural and spatial characteristic of the captured image, the proposed solution avoided false color shifts and moire noise, produced visually pleasing demosaicked images, and outperformed leading demosaicking solutions both objectively and subjectively.

6. REFERENCES

[1] K. Parulski and K. E. Spaulding, "Color image processing for digital cameras," in *Digital Color Imaging Handbook*, (eds.) G. Sharma, CRC Press, Boca Raton, FL., pp. 728-757, 2002.

[2] B. K. Gunturk, J. Glotzbach, Y. Altunbasak, R. W. Schaffer, and R. M. Murserau, "Demosaicking: color filter array interpolation," IEEE Signal Processing Magazine, vol. 22, pp. 44-54, January 2005.

[3] B. Gunturk, Y. Altunbasak, and R. Mersereau, "Color plane interpolation using alternating projections," *IEEE Trans. Image Processing*, vol. 11, pp. 997-1013, September 2002.

[4] W. Lu and Y. P. Tang, "Color filter array demosaicking: new method and performance measures," *IEEE Trans. Image Processing*, vol. 12, pp. 1194-1210, October 2003.

[5] R. Lukac and K. N. Plataniotis, "Data-adaptive filters for demosaicking: A framework," *IEEE Trans. Consumer Electronics*, vol. 51, pp.560-570, May 2005.

[6] L. Chang and Y. P. Tang, "Effective use of spatial and spectral correlations for color filter array demosaicking," *IEEE Trans. Consumer Electronics*, vol. 50, pp. 355-365, May 2004.
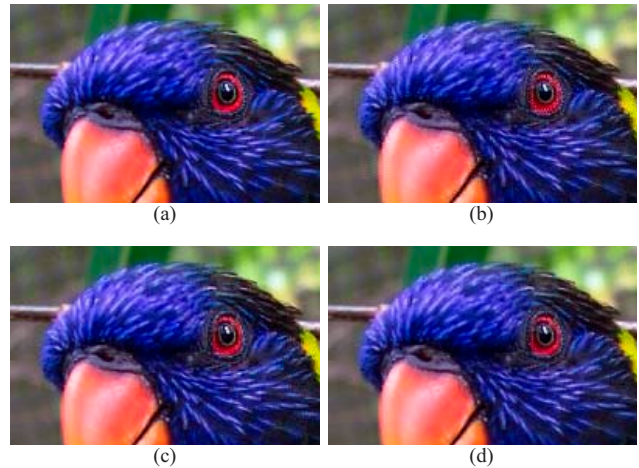
[7] R. Lukac, K. N. Plataniotis, D. Hatzinakos, and M. Aleksic, "A novel cost effective demosaicing approach," *IEEE Trans. Consumer Electronics*, vol. 50, pp. 256-261, February 2004.

[8] X. Wu and N. Zhang, "Primary-consistant soft-decision color demosaicking for digital cameras," *IEEE Trans. Image Processing*, vol. 13, pp. 1263-1274, September 2004.

[9] D. D. Muresan and T. W. Parks, "Demosaicing using optimal recovery," *IEEE Trans. Image Processing*, vol. 14, pp. 267-278, February 2005.

[10] R. Lukac and K.N. Plataniotis, "A vector spectral model for digital camera image processing," *IEEE Trans. Circuit and Systems for Video Technolog*, submitted, March 2005.

[11] R. Lukac, B. Smolka, K. Martin, K.N. Plataniotis, A.N. Venetsanopulos, "Vector filtering for color imaging," *IEEE Signal Processing Magazine*, vol. 22, pp. 74-86, January 2005.

[12] P. E. Trahanias, D. Karakos, and A. N. Venetsanopoulos, "Directional processing of color images: theory and experimental results," *IEEE Trans. Image Processing*, vol. 5, pp. 868-881, June 1996.

[13] B. Tang, G. Sapiro, and V. Caselles, "Color image enhancement via chromaticity difussion," *IEEE Trans. Image Processing*, vol. 10, pp. 701-707, May 2001.

[14] B.E. Bayer, "Color imaging array," *U.S. Patent 3 971 065*, July 1976.

[15] D. R. Cok, "Signal processing method and apparatus for producing interpolated chrominance values in a sampled color image signal," *U.S. Patent 4 642 678*, February 1987.

[16] J. Adams, "Design of practical color filter array interpolation algorithms for digital cameras," *Proceedings of the SPIE*, vol. 3028, pp. 117-125, February 1997.

[17] R. Lukac, K. Martin, and K.N. Plataniotis, "Demosaicked image post-processing using local color ratios," *IEEE Trans. Circuit and Systems for Video Technology*, vol. 14, pp. 914-920, June 2004.

[18] R. Lukac and K. N. Plataniotis, "Normalized color-ratio modelling for CFA interpolation," *IEEE Trans. Consumer Electronics*, vol. 50, pp. 737-745, May 2004.

[19] B. Wandell, "S-CIELAB: A spatial extension of the CIE L*a*b* DeltaE color difference metric." [Online] http://white.stanford.edu/∼brian/scielab/